metals

MDPI

Article

Regulation of Microstructure to Optimize Mechanical Properties of Ti-15Mo-3Al-2.7Nb-0.2Si via Solution-Duplex Ageing

Xudong Kang [1], Hanyu Jiang [1], Zhaoxin Du [1,2,3,*], Tianhao Gong [1,3], Jingwen Liu [1], Wenxia Guo [4], Jun Cheng [5], Jingshun Liu [1,2] and Guowei Li [1]

[1] School of Materials Science and Engineering, Inner Mongolia University of Technology, Hohhot 010051, China; kangxudong1995@163.com (X.K.)
[2] Collaborative Innovation Center of Non-Ferrous Metal Materials and Processing Technology Co-Constructed by the Province and Ministry, Inner Mongolia University of Technology, Hohhot 010051, China
[3] Inner Mongolia Key Laboratory of Light Metal Materials, Inner Mongolia University of Technology, Hohhot 010051, China
[4] Engineering Training and Teaching Department, Inner Mongolia University of Technology, Hohhot 010051, China
[5] Northwest Institute for Non-Ferrous Metal Research, Shaanxi Key Laboratory of Biomedical Metal Materials, Xi'an 710016, China
* Correspondence: duzhaoxin@163.com

Abstract: The production of alloys with high strength and toughness concurrently is still a difficult challenge. Here, we designed a simple solution-ageing heat treatment system to control the morphology and density of α in Ti-15Mo-3Al-2.7Nb-0.2Si via different heat treatment temperatures. The experimental results show that Ti-15Mo-3Al-2.7Nb-0.2Si exhibits a synergistic combination of tensile strength (1364 MPa), plasticity (7.8% elongation), and fracture toughness (101 MPa·m$^{1/2}$) through solutions in the α/β biphasic region and duplex ageing. Notably, the strength of the alloy after the second step of the ageing process is increased by 15% compared with that after the first step of the ageing process. However, there is less than a 5% reduction in the fracture toughness. TEM observations show that the matrix continues to precipitate denser secondary α during duplex ageing, which causes the strength to increase significantly and causes the fracture toughness to weaken. Our work may provide a novel method to optimize the mechanical properties of alloys by controlling the precipitates.

Keywords: β titanium alloy; heat treatment; duplex ageing; tensile properties; fracture toughness

check for updates

Citation: Kang, X.; Jiang, H.; Du, Z.; Gong, T.; Liu, J.; Guo, W.; Cheng, J.; Liu, J.; Li, G. Regulation of Microstructure to Optimize Mechanical Properties of Ti-15Mo-3Al-2.7Nb-0.2Si via Solution-Duplex Ageing. *Metals* **2023**, *13*, 869. https://doi.org/10.3390/met13050869

Academic Editor: Evgeny A. Kolubaev

Received: 12 March 2023
Revised: 11 April 2023
Accepted: 27 April 2023
Published: 29 April 2023

Copyright: © 2023 by the authors. Licensee MDPI, Basel, Switzerland. This article is an open access article distributed under the terms and conditions of the Creative Commons Attribution (CC BY) license (https://creativecommons.org/licenses/by/4.0/).

1. Introduction

Metastable β titanium alloy has not only high strength, good corrosion resistance, and excellent fatigue resistance but also good toughness. Thus, it is widely used in various applications in the aerospace field, such as in aircraft engines, aircraft parts, and rockets [1–3]. For most structural materials, the properties of strength and toughness are usually mutually exclusive [4]. Moreover, researchers have been able to control the size, content, and distribution of the phases in the tissues through a variety of strengthening strategies to achieve strengthening and toughening effects [5–8].

In the past few decades, many studies have focused on the effect of different solutions and ageing processes on the microstructure and properties of β titanium alloys. The most common process is single ageing, in which changes in the secondary α phase correspond to a single property. For example, Chen et al. [9] found from the effect of a single ageing temperature on the morphology of the secondary α phase that the size of the secondary α phase increased with the increasing ageing temperature; this led to a decrease in strength and an increase in ductility. Decreasing the size of the secondary α phase or increasing

the volume fraction would improve the strength of the alloy. Because the larger secondary α phase is more likely to activate the twin system than the smaller secondary α phase, the strength of the alloy will decrease, and the plasticity will increase. However, this law is only considered for different single ageing temperatures [10]. The good crack propagation resistance can be attributed to crack deflection, long secondary cracks, and tortuous crack paths induced by the coarse secondary α phase [11], which was beneficial to the improvement of ductility and fracture toughness. Generally, duplex ageing has unique advantages. For example, Santhosh et al. [12] found that duplex ageing results in a smaller size and higher density α phase precipitation, and the hardness and strength of metastable β-type Ti-15V-3Cr-3Al-3Sn alloys were obviously higher than that of single ageing. Ren et al. [13] obtained a small and uniform size secondary α phase through a low-high temperature rising-order duplex ageing method; although the strength increased significantly, the plastic loss was large. In conclusion, the change in a single microstructure component can only unilaterally improve the strength or plasticity, and the improvement in strength is often accompanied by a loss in plasticity.

This strategy of low-high temperature duplex ageing with ascending order used precursor-assisted nucleation to reduce the size of the secondary α phase to achieve a high yield strength [14,15]; however, the plasticity and toughness were poor. Our previous study also found that the alloy had significant strength but less plastic loss after high-low temperature descending order duplex ageing [16] because the large size of the secondary α phase was formed by high-temperature ageing (similar to single ageing), which ensures good plasticity. An alloy with excellent comprehensive mechanical properties can be obtained by reasonably adjusting the duplex ageing process with a descending sequence and strengthening the alloy with less plastic loss [17]. Fan et al. [18] showed that β titanium alloy had a high fracture toughness value under a β solution followed by slow cooling and then an ageing heat treatment process while maintaining good plasticity and a certain strength. For fracture toughness, the coarser and longer intragranular α and more multidirectional arrangement of the colony of α lamellae led to a more tortuous crack propagation path and higher fracture toughness.

In addition, researchers found that the α phase microstructure with a scale gradient obtained during heat treatment was conducive to improving the comprehensive matching of the strength and toughness of titanium alloys [19,20]. For titanium alloys, the multiscale lamella structure exhibits an improved strength-fracture toughness combination that is better than that of the single lamella structure and bimodal structure, which is mainly attributed to the more tortuous crack propagation path caused by the multiscale lamella microstructure [21]. Zhu et al. [22] found a hierarchical microstructure consisting of an elongated primary α phase, submicron α-rod, and nanoscale α-platelets, which possess a good combination of strength and plasticity. The high strength of the alloy was mainly attributed to the nanoscale secondary α phase with a highly defective substructure, while the improved ductility resulted from a more effective strain partition and compatibility inside the hierarchical α-structure.

Taking Ti-15Mo-3Al-2.7Nb-0.2Si titanium alloy (hereinafter collectively referred to as TB8) as the research object, a multistage heat treatment strategy is designed to achieve the best balance of strength and plastic toughness while adjusting the heat treatment process of the solution treatment and duplex ageing in descending order. After the solution treatment in the α/β region and β region, the microstructure evolution of the alloy was studied at different ageing temperatures in detail to obtain a kind of microstructure composed of different scales of secondary α phases. The relationship between the microstructure and mechanical properties was further studied, and the relationship between the microstructure, strength, and fracture toughness of metastable β alloy was discussed.

2. Materials and Methods

TB8 titanium alloy was prepared by electric arc melting, and its chemical constituents are shown in Table 1. After forging, a bar with a diameter of 73 mm was obtained. The β-transus temperature of the alloy, determined by the metallographic method, is (810 ± 5) °C. Figure 1 shows the initial structure of the TB8 alloy consisting of a large amount of equiaxed primary α phase distributed in the β matrix.

Table 1. Chemical constituents of the TB8 alloy (wt. %).

Element	Mo	Al	Nb	Si	O	Fe	H	N	C	Ti
TB8	15	3.32	2.51	0.164	0.089	0.104	0.001	0.0092	0.0097	Bal.

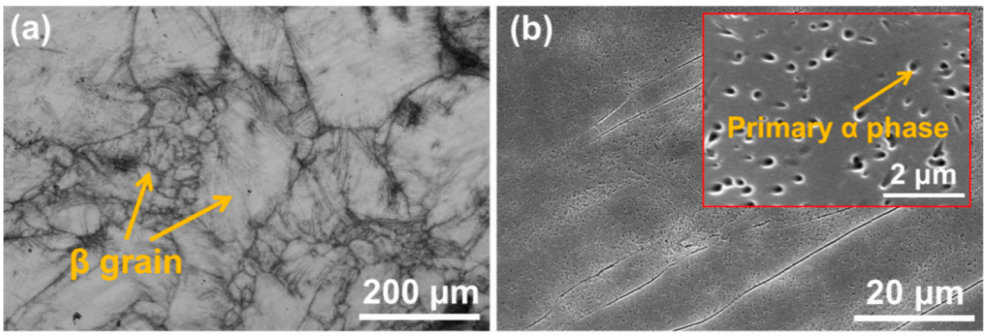


Figure 1. Initial microstructure of the TB8 alloy: (**a**) metallographic microstructure; (**b**) scanning microstructure.

Figure 2 shows a sketch map of the heat treatments of the TB8 alloy. Solution treatments were conducted at 750 °C (α/β field), 790 °C (α/β field near the phase transition point), and 830 °C (β field) for 0.5 h, followed by air cooling. The first-step ageing treatments were carried out at 520 °C for 4 h and then treated by air cooling. The second-step ageing treatments were conducted at 300 °C, 350 °C, and 400 °C for 4 h, followed by air cooling.

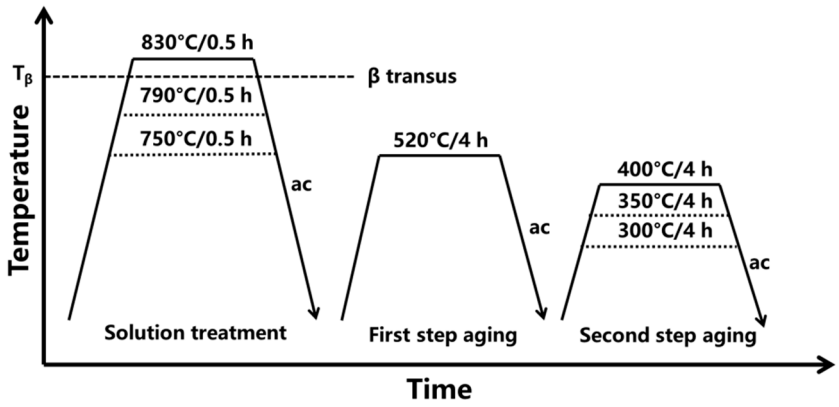


Figure 2. Schematic diagram of the heat treatment process of TB8 alloys.

The microstructure evolution was characterised by scanning electron microscopy (SEM) and transmission electron microscopy (TEM). Before SEM observation on an FEI Quanta 650 FEG machine, the samples were mechanically polished and corroded in Kroll reagent (3 mL HF, 7 mL HNO_3 and 90 mL H_2O). TEM observations were performed on a Talos 200X instrument. The TEM samples were first ground and polished to 100 μm thickness and then punched into 3 μm diameter disks, which were finally perforated in an electrolyte of 5% perchloric acid, 35% butanol, and 60% methanol at 228 K by double-jet

electrochemical polishing. The XRD samples were analysed by a D/MAX-2500/PC X-ray diffractometer at a scanning angle of 20–80°.

The tensile specimen with a circular section of 10 mm in diameter (Figure 3a) was subjected to room temperature tensile testing at a constant crosshead speed of 1 mm/min on an electronic universal testing machine (LX-E19-002). To ensure repeatability, each value is an average of three measurements. The fracture toughness was tested on an electrohydraulic servo fatigue tester (LX-E19-114) using three-point bending specimens (Figure 3b). After the test, the fracture morphology was observed by SEM.

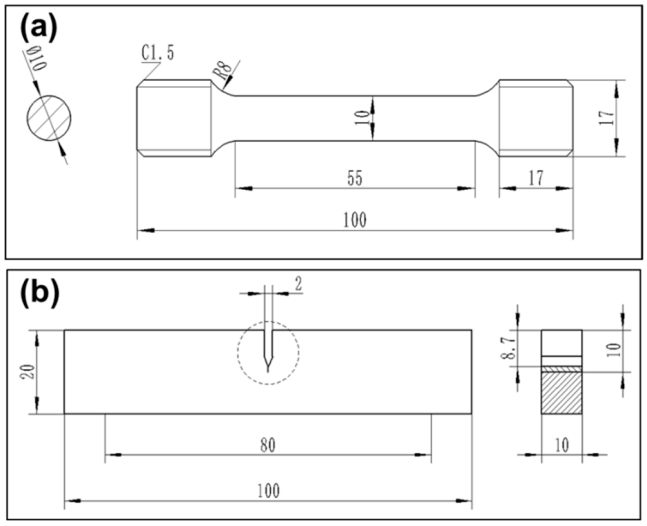


Figure 3. Specimen dimensions for tensile and fracture testing: (**a**) tensile specimens; (**b**) three-point bending experiments (Unit: mm).

Specimens with a width (W) of 20 mm and a thickness (B) of 10 mm are used for fracture toughness testing. The fatigue crack is prefabricated on the width (W) and the fatigue crack length (a). The load (P)-displacement (Δ) curve was recorded by a recorder, and the conditional load F_Q was calculated. The K_Q (the conditional value of K_{IC}) was calculated as shown in Formulas (1) and (2):

$$K_Q = f\left(\frac{a}{W}\right) \times \left(\frac{F_Q S}{BW^{3/2}}\right) \tag{1}$$

$$f\left(\frac{a}{W}\right) = 3\left(\frac{a}{W}\right)^{1/2} \times \frac{1.99 - \left(\frac{a}{W}\right)\left(1 - \frac{a}{W}\right)\left[2.15 - 3.93\left(\frac{a}{W}\right) + 2.70\left(\frac{a}{W}\right)^2\right]}{2\left(1 + \frac{2a}{W}\right)\left(1 - \frac{a}{W}\right)^{3/2}} \tag{2}$$

If Formula (3) is true, the obtained K_Q value is substituted into the following discriminant Formula (4). If all the formulas are met, then K_Q is equal to K_{IC}. Otherwise, the experiment is not an effective K_{IC} test.

$$\frac{F_{max}}{F_Q} \leq 1.10 \tag{3}$$

$$B \geq 2.5\left(\frac{K_Q}{R_{P0.2}}\right)^2, a \geq 2.5\left(\frac{K_Q}{R_{P0.2}}\right)^2, W - a \geq 2.5\left(\frac{K_Q}{R_{P0.2}}\right)^2 \tag{4}$$

where F_{max} is the maximum load, F_Q is the conditional load, and $R_{P0.2}$ is the yield strength of the sample.

The effective K_{IC} value is a material constant that reflects the fracture resistance of the material. The prerequisite is that the thickness is large enough to meet the plane strain state. The K_Q value reflects the fracture resistance of the material under a given thickness and

can also represent fracture toughness to a certain extent. The whole test process completely conforms to the national standard «GB/T4161-2007 Metallic Materials-Determination of plane-strain fracture toughness».

3. Results

3.1. Microstructure and Tensile Properties of the Solution-Treated Alloy

Figure 4 shows the corresponding XRD pattern of the alloy after solution treatment. It can be seen that there are α and β phases after solution treatment in the α + β region and a single β phase when solution treatment occurs in the β region. Figure 5 shows SEM and EBSD images of TB8 alloys after solution treatment. The microstructures composed of equiaxed and rod-shaped primary α phases (α_p) were distributed in the β matrix after solution treatment in the α/β region and single β grains after solution treatment in the β region. The amount of α_p decreases with an increasing solution temperature, and α_p disappears completely until 830 °C. Observing the EBSD maps of Figure 5b,d,f, it can be found that the size of β grains grows with an increasing solution temperature.

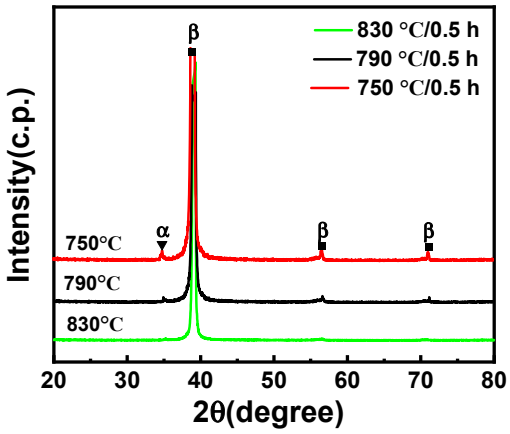


Figure 4. X-ray diffraction pattern of the solution-treated alloy.

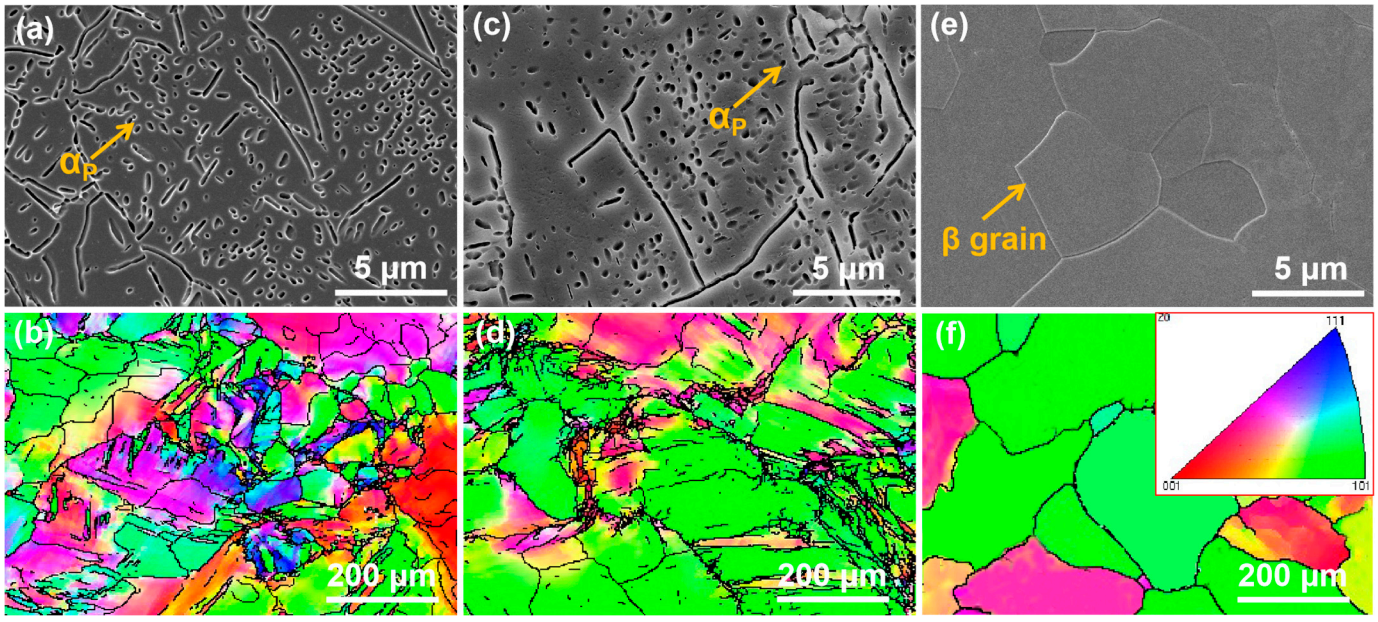


Figure 5. SEM and EBSD images of TB8 alloys after solution treatment: (**a**,**b**) solution treatment at 750 °C; (**c**,**d**) solution treatment at 790 °C; (**e**,**f**) solution treatment at 830 °C.

Figure 6 shows the tensile properties of the solution-treated TB8 alloy. The tensile strength (Rm) and yield strength (Rp) show a decreasing trend (Figure 6a), while the elongation (A) and reduction of the area (Z) show a slightly rising trend (Figure 6b) with an increasing solution temperature. The reduction in strength is mainly attributed to the reduction in the size and number of α_p. However, the slight increase in elongation and section reduction is the result of a combination of decreasing α_p and the growth of β grain size. For strength, on the one hand, Figure 5 shows that the amount of α_p decreases with increasing solution temperature, which leads to the reduction of the α/β phase interface and the weakening of the strengthening effect for the second phase [16]. On the other hand, the change in the tensile properties is related to the fine grain strengthening mechanism [23]. The EBSD maps in Figure 5 show that the β grain size gradually grows with an increasing solution temperature, which leads to the minimum strength of the β region solution-treated alloy. For plasticity, the increasing content of the β matrix with the BCC structure makes more slip systems available for the alloy to slip during plastic deformation, thus improving the plastic deformation capacity of the alloy [24] and resulting in the maximum plasticity of the β region solution-treated alloy. In addition, from another point of view, the higher solution temperature gives the alloy a larger recrystallization driving force, so the 830 °C solution treatment of alloy recrystallization is more complete, resulting in a decrease in strength.

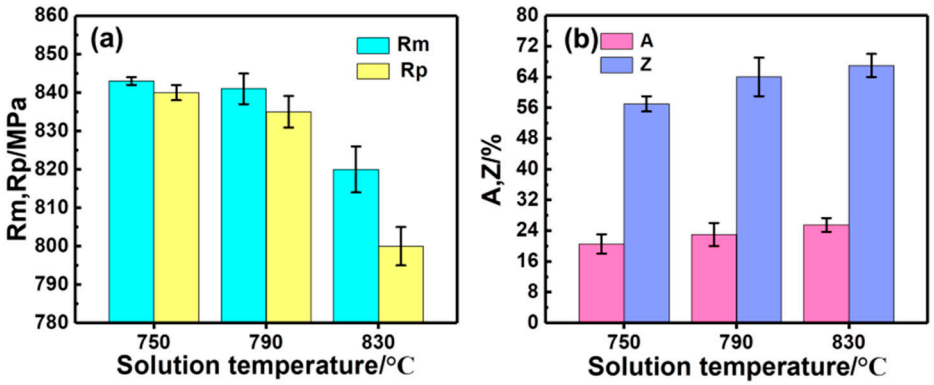


Figure 6. Tensile properties of the TB8 alloy after solution treatment: (**a**) tensile strength (Rm) and yield strength (Rp); (**b**) elongation (A) and reduction of area (Z).

3.2. Microstructure of the Duplex-Aged Alloys

Figure 7 shows SEM images of the TB8 alloy after single and duplex ageing. A large amount of needle-like α phases precipitated in the β matrix during the first step of ageing at 520 °C (Figure 7a,e,i). At the same time, it can be found that there are large amounts of α_p and a large number of α_S after solution treatment at 750 °C plus ageing (Figure 7a), a small amount of α_p and a large number of α_S after solution treatment at 790 °C plus ageing (Figure 7e), and there is only a large amount of α_S after solution treatment at 830 °C plus ageing (Figure 7i). After the duplex ageing, finer α_S precipitates between the first precipitated α_S (Figure 7c,g,k). The quantity and density of α_S gradually increase with an increasing second step ageing temperature, and α_S has the largest number and the highest density of precipitation when ageing at 400 °C (Figure 7h). This is because the increase in temperature accelerates the diffusion rate, which is beneficial to the precipitation and faster growth of the α phase [25]. Figure 8 shows the quantitative analyses of the corresponding SEM images; the result indicated that more α_p with larger size appeared in the single ageing process, and with the increase in duplex ageing temperature, the volume fraction of α_p decreased from 6.38% to 1.77%, and the length decreased from 0.82–0.38μm. Figure 9 shows the size distribution and volume fraction of α_p with different heat treatments.

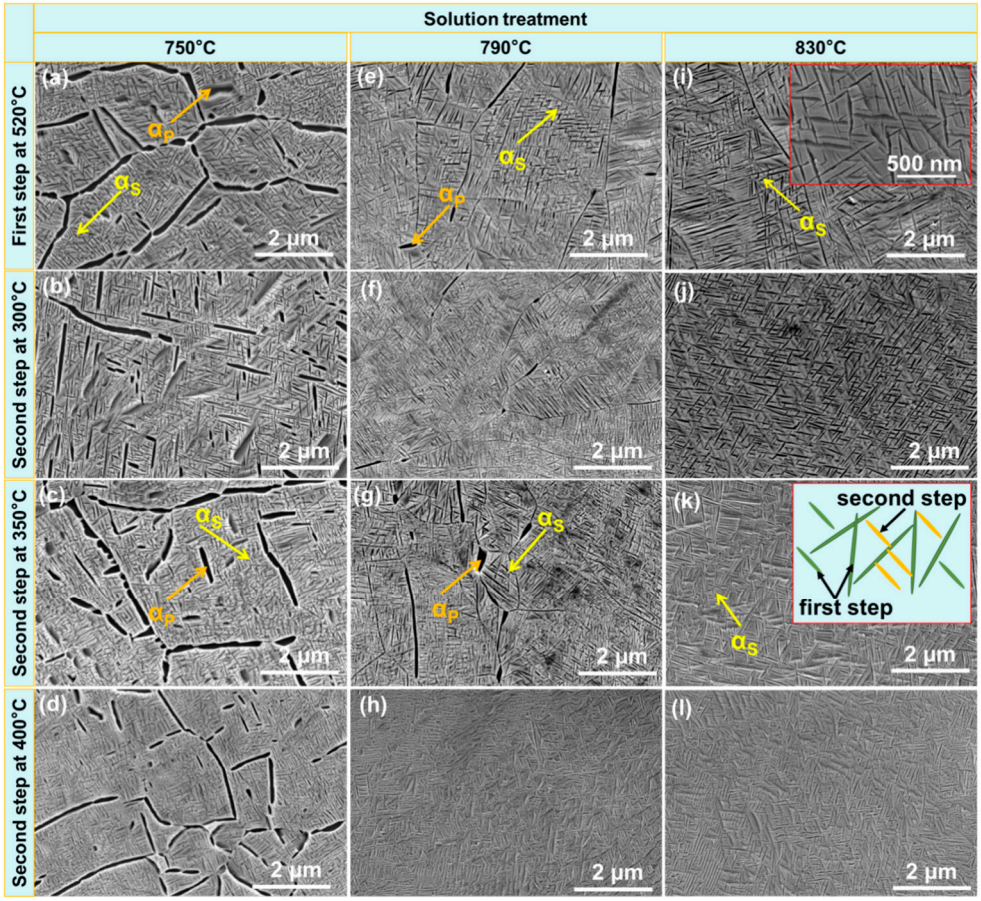


Figure 7. SEM images of the TB8 alloy after solution treatment at different temperatures and duplex ageing: (**a**–**d**) 750 °C; (**e**–**h**) 790 °C; (**i**–**l**) 830 °C.

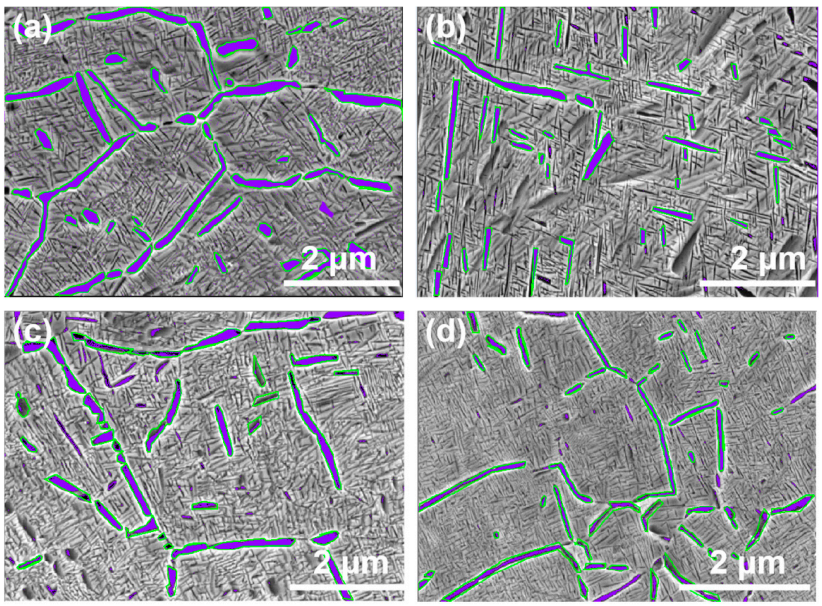


Figure 8. Quantitative analyses of the corresponding SEM images, with the purple representing α_p. (**a**) 750 °C + 520 °C, (**b**) 750 °C + 520 °C + 300 °C, (**c**) 750 °C + 520 °C + 350 °C, (**d**) 750 °C + 520°C + 400 °C.

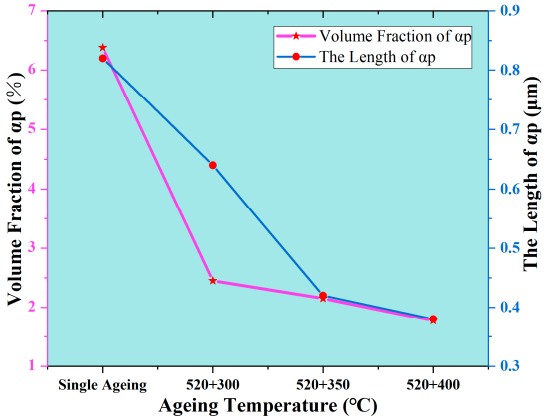


Figure 9. Size distribution and volume fraction of α_p with different heat treatments.

3.3. Mechanical Properties of Aged Alloy

Figure 10 shows the mechanical properties of the TB8 alloy after ageing. For the first step of ageing, the alloy obtained moderate strength and good ductility and fracture toughness. As shown in Figure 10a–c, the second step of ageing on the basis of the completion of the first step of ageing can further improve the strength while causing a reduction in plasticity and fracture toughness. During the second step of the ageing process, the tensile strength and yield strength of the alloy gradually increase (Figure 10a,d,g), while the elongation and reduction of the area gradually decrease with the increasing quantity and density of α_S (Figure 10b,e,h). The fracture toughness also decreases gradually with an increasing ageing temperature (Figure 10c,f,i).

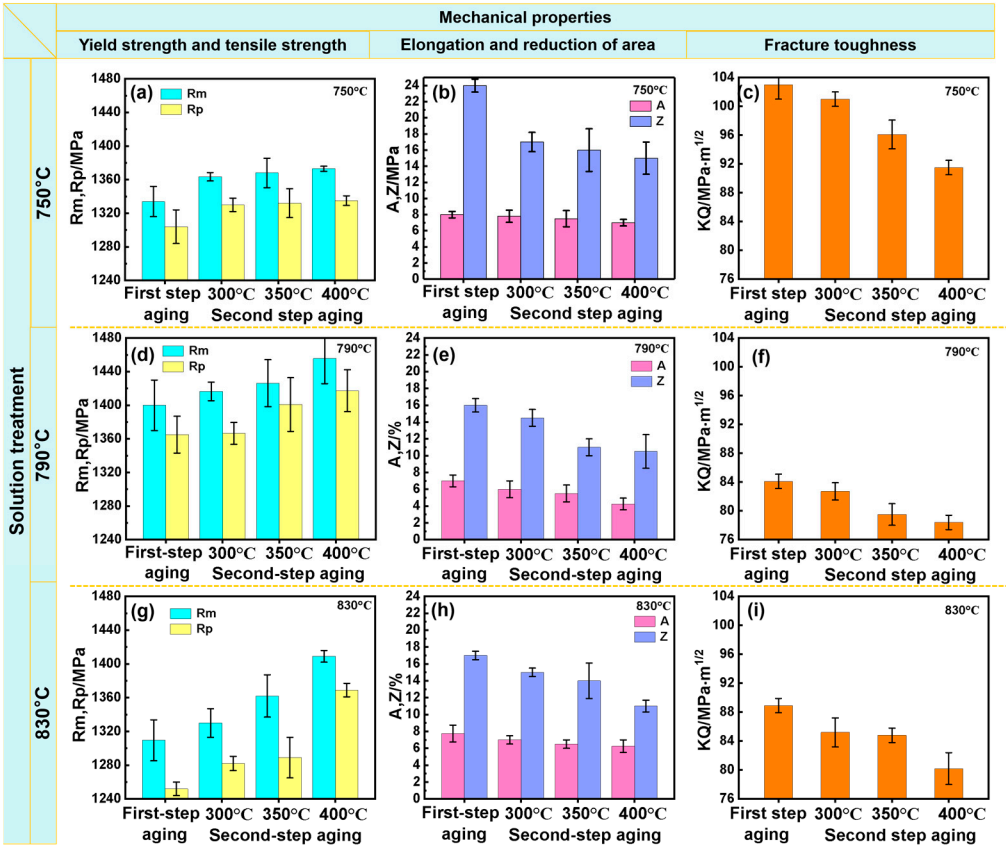


Figure 10. Mechanical properties of the TB8 alloy after solution treatment at different temperatures and duplex ageing: (**a**–**c**) 750 °C; (**d**–**f**) 790 °C; (**g**–**i**) 830 °C.

4. Discussion

4.1. Effect of the Solution Temperature on the Tensile Properties of Aged Alloys

Figure 11 shows the effect of solution temperature on the mechanical properties of aged alloys. It is shown that the tensile strength and yield strength of the alloy treated at 790 °C are higher than those of the other two alloys treated at solution temperature. The plasticity of the alloy is just opposite to its strength. In addition, the fracture toughness of the alloy treated at 750 °C is obviously better than that of the other two samples. The increase in alloy strength after solution treatment at 790 °C is mainly due to the number of αs, which is affected by the number of αp and the size of β grains after solution treatment in the α + β region. The α_p formed during the α/β solution treatment can increase the stability of the β matrix and reduce the driving force of α_S in the subsequent ageing process [26,27]. Due to the small size of β grains and large amount of α_p (Figure 7a), the alloy of the solution treated at 750 °C plus ageing has a small amount of α_S compared with that at 790 °C. More α_S precipitation leads to an increase in the amount of α/β phase interfaces, which can effectively block dislocation movement during tensile deformation [28], thus leading to an increase in strength and a decrease in plasticity.

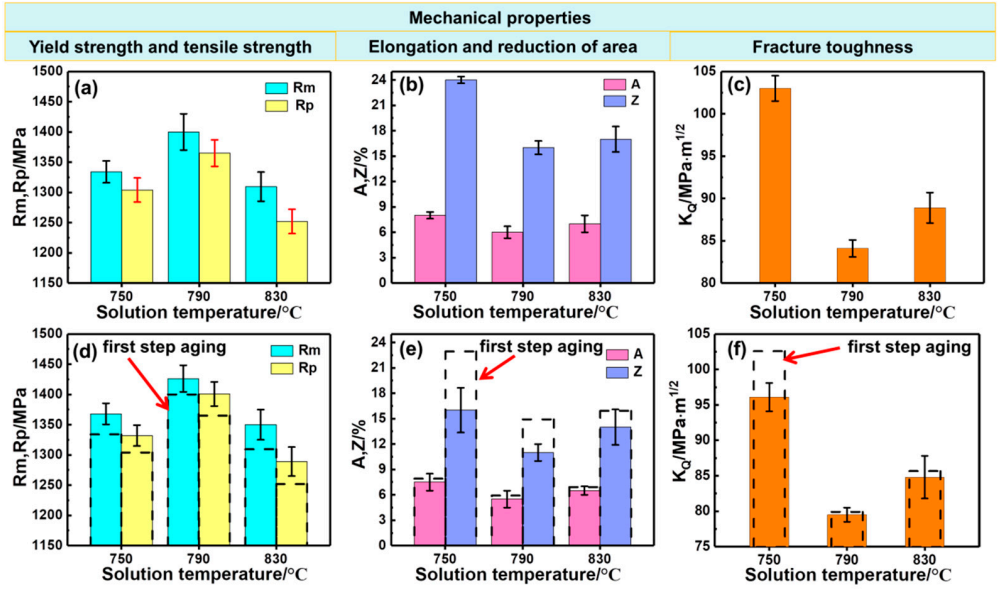


Figure 11. Effect of the solution temperature on the mechanical properties of aged alloys: (**a**–**c**) first step of ageing at 520 °C; (**d**–**f**) duplex ageing at 520 °C and 350 °C.

The reason for the sudden decrease in strength and the sudden increase in plasticity and fracture toughness is that the β solution treatment results in coarse β grains, the least stable β matrix, and the greatest driving force for growth [29]. α_S with a sparse distribution tends to form during ageing. Therefore, the alloy of the solution treated at 830 °C plus ageing has a small number of α_S compared with that at 790 °C (Figure 7i). In addition, the reason can also be attributed to the decrease in residual internal defects and stresses associated with the growth of β grains [30].

4.2. Effect of the Solution Temperature on the Fracture Toughness of Aged Alloys

The fracture toughness of the aged alloy has the same trend as the plasticity in that the fracture toughness initially decreases and then increases with increasing solution temperatures (Figure 11c). To explain the mechanism of the fracture toughness change, the crack propagation path and the fracture morphology are observed and analysed.

Figure 12 shows that the deflection angle of the crack propagation path decreases for the alloy aged in the first step and then increases with an increasing solution temperature, which corresponds to the change trend of the fracture toughness. According to the crack

deflection angle, the crack and the area formed by the crack path and the midline in the figure, and the crack propagation path after the solution treatment at 750 °C is the most tortuous, followed by the solution at 830 °C. Moreover, the crack path after the treatment solution at 790 °C is slightly flat. During solution treatment from 750 °C to 790 °C plus ageing, the amount of α_p decreases, and the amount of α_S increases (Figure 12d,e). α_p with an equiaxed or thick lamella also plays an important role in the toughness [31]. The cracks initiate at the interior of α_p, the crack propagation rate slows down, and the crack propagation path increases with an increasing α_p, which consumes more energy and improves the fracture toughness of the alloy [32,33]. After solution treatment in the β region plus ageing, the fracture toughness increases again, which is attributed to coarser β grains resulting in a decrease in the amount of α_S (Figure 12f). Shi et al. [34] found that long and thick α platelets can lead to a rough crack front geometry, which makes it have higher crack propagation resistance, and therefore, its crack propagation path is more tortuous. There are studies that show that the crack path tortuosity also has a positive correlation with the β grain size; that is, a coarse β grain size is beneficial for improving the fracture toughness [31,35].

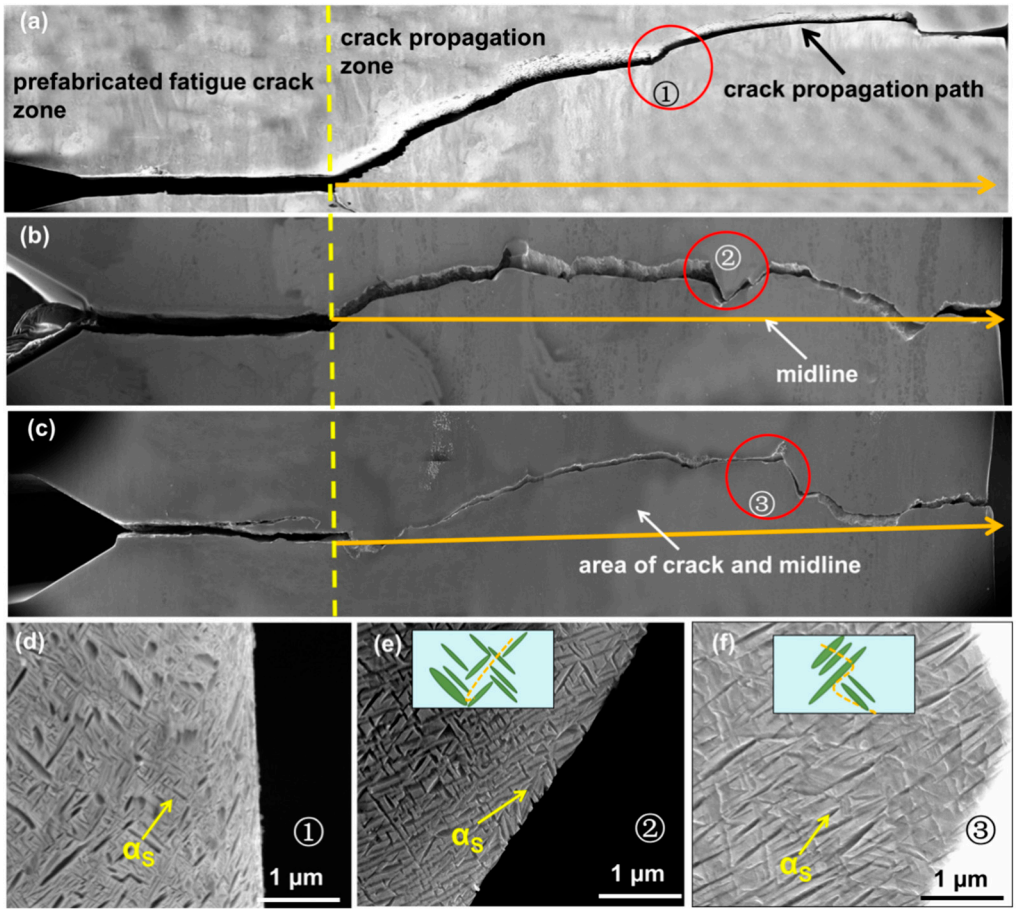


Figure 12. Crack propagation path of the TB8 alloy after solution treatment at different temperatures and the first step of ageing: (**a**) 750 °C + 520 °C; (**b**) 790 °C + 520 °C; (**c**) 830 °C + 520 °C; (**d**) microstructure in Region 1; (**e**) microstructure in Region 2; (**f**) microstructure in Region 3.

On the other hand, the microstructure close to the crack in the alloy can accurately reflect the crack deflection angle of the crack propagation path, and the complicated microstructure corresponds to the complex crack propagation path; thus, the fracture toughness is the highest in this scenario.

Figure 13 shows the fracture morphologies in a mixed mode of trans-granular fracture and intergranular fracture, mainly distributed with dimples and tearing edges (Figure 13b). The fracture morphology of the aged alloy is the roughest when the solution is treated at 750 °C, while that of the solution at 790 °C is slightly flat. Ghosh et al. [36] showed that the fracture mode of samples with high fracture toughness was dimple fracture accompanied by secondary cracking, while that of samples with low fracture toughness was mixed mode (dimple fracture and cleavage fracture). In addition, Huan Wang et al. [37] showed that the desired microstructure responsible for high fracture toughness should consist of a discontinuous grain boundary α film, large β grains and a uniform α_p phase with highly misoriented boundaries. Therefore, alloys with a large number of α_p, large size and a large amount of α_S obtained by solution treatments at the α/β region plus ageing will obtain the best match of strength and toughness (Figure 7a).

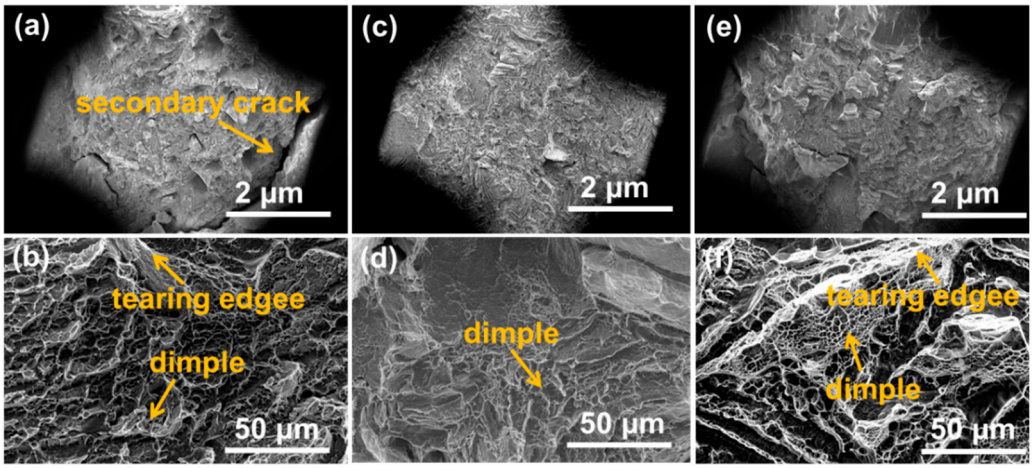


Figure 13. Fracture morphologies for fracture toughness of the first-step aged alloy: (**a**,**b**) 750 °C + 520 °C; (**c**,**d**) 790 °C + 520 °C; (**e**,**f**) 830 °C + 520 °C.

4.3. Effect of Duplex Ageing on the Microstructure and Mechanical Properties

TEM images of the alloy after solution treatment at 830 °C and duplex ageing (Figure 12) were used to further illustrate the change in the microstructure during the first and second steps of ageing. After the first step of ageing, a large amount of α_S precipitates in the microstructure (Figure 14a). Then, during the second step of ageing, finer α_S precipitates between the first precipitated α_S (Figure 14c). α_S with a step distribution is formed in the microstructure through duplex ageing, which uses a temperature difference to cause a driving force difference. It is well known that the phase transition is achieved by the migration of atomic vacancies. Therefore, at a higher ageing temperature, the increase in the frequency and rate of thermal motion of atoms leads to an increase in the concentration of vacancies in the matrix so that the driving force of the phase transition will decrease, but the thermal motion of the atoms increases, eventually resulting in less α_S precipitation and a larger size [30]. Low-temperature ageing exhibits opposite characteristics, so more phases with small sizes are formed.

Figure 15 shows the comparison of the mechanical properties under different manual processes. The alloy has a moderate strength level and excellent ductility after solution treatments. The first step of ageing can improve the strength while causing a reduction in plasticity, and the second step of ageing can further improve the strength of the alloy. The α_S produced by duplex ageing is denser, which exhibits precipitation strengthening and dispersion strengthening [38]. During the tensile deformation of the specimen, the α/β phase interface can be used as a barrier to the dislocation slip, and the increase in the amount and the decrease in the size of α_S will improve the strength of the alloy [39]. An increase in the strength is accompanied by a loss of plasticity and fracture toughness, but

the extent of the decrease is small after the second step of ageing, which is the reason for α_S to have a step distribution and a limited amount precipitated in the second step of ageing.

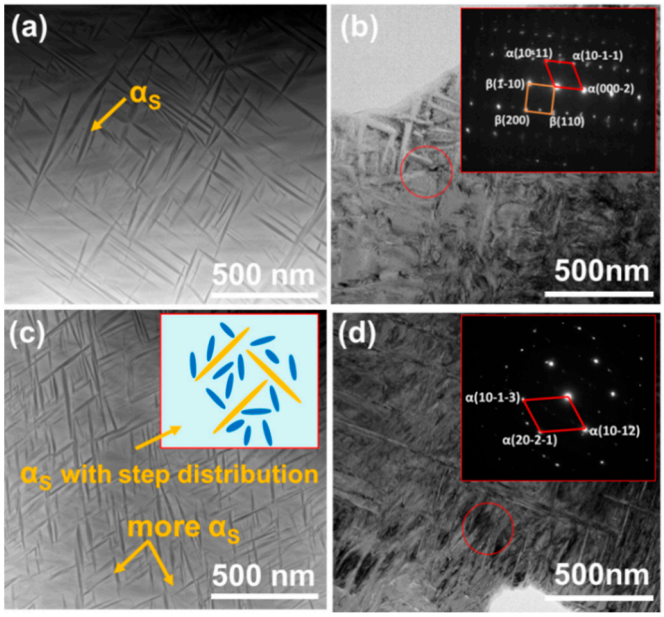


Figure 14. TEM morphology comparison for the TB8 alloy of solution treatments at 830 °C and duplex ageing: (**a**,**b**) first-step ageing at 520 °C; (**c**,**d**) first-step ageing at 520 °C plus second-step ageing at 350 °C.

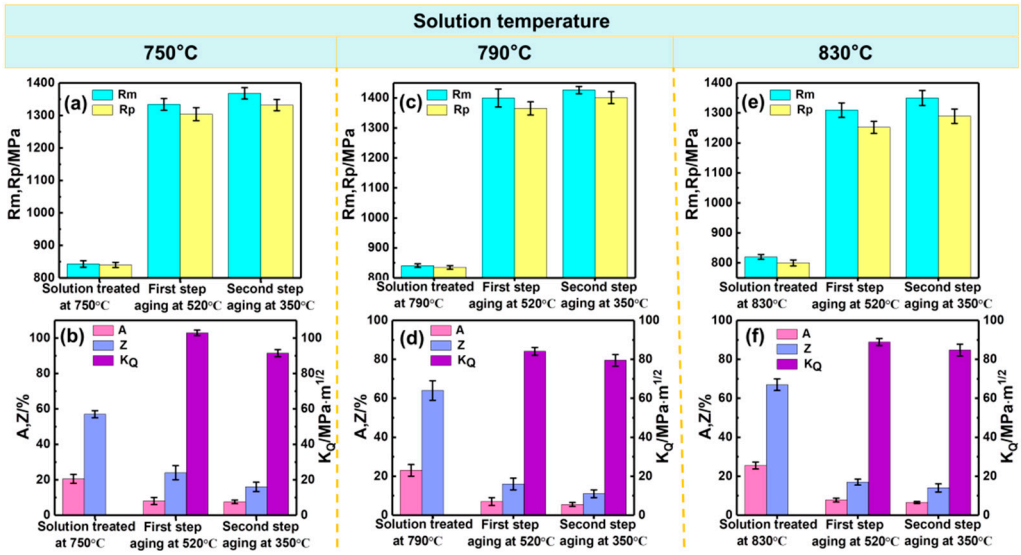


Figure 15. Mechanical properties of alloy in different solution temperatures after ageing treatment: (**a**,**b**) 750 °C; (**c**,**d**) 790 °C; (**e**,**f**) 830 °C.

For fracture toughness, as explained by the crack propagation path in Figure 16, it can be seen that the α phase of the first step of ageing has a deflection effect on the main crack, forming a complicated crack propagation path (Figure 16b), and the fracture morphology is characterized by dimples (Figure 16c). In the second step of ageing, more α phase precipitates, the crack propagation path is relatively flat (Figure 16e), and the fracture morphology is characterized by dimple and cleavage platforms (Figure 16f). Ghosh et al. [36] showed that the long and thick lamellar α phase made it difficult for the crack to advance through the cutting mechanism, and the crack would be more inclined to bypass the lamellar α

phase to advance, resulting in complicated path expansion. Mine et al. [40] also pointed out that the fine α phase could not affect the growth of the main crack, and the crack would be more inclined to cut through the α phase and expand forward, resulting in a very flat crack growth path. The higher the bending degree of the crack propagation path is, the higher the fracture toughness of the alloy [25]. In conclusion, cracks tend to propagate at the interior of the α phase (Figure 16a), while cracks tend to propagate at the fine α/β interface (Figure 16d). The α_S with step distribution precipitates after duplex ageing, but the first step of ageing contains a certain amount of α phase and results in higher fracture toughness than the second step of ageing, which contains a finer α phase.

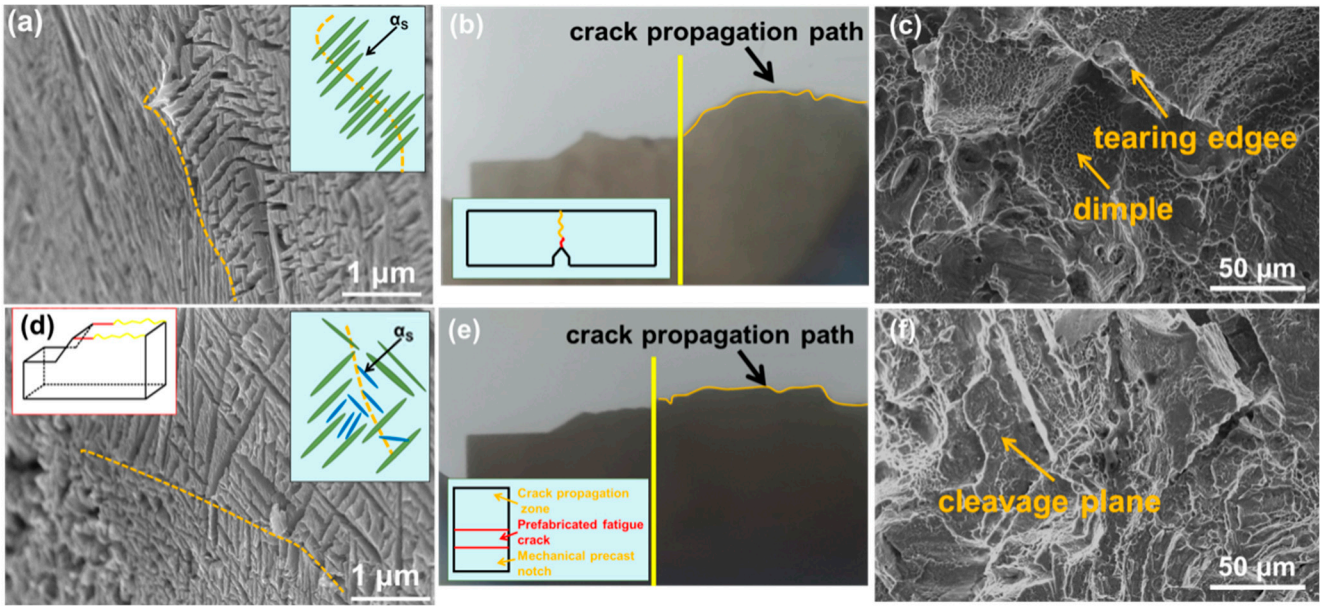


Figure 16. Crack propagation path of the TB8 alloy of solution treatments at 830 °C and duplex ageing: (**a**–**c**) first-step ageing at 520 °C; (**d**–**f**) second-step ageing at 350 °C.

4.4. Combination Properties after the Solution-Duplex Ageing

Mechanical properties after the solution-duplex ageing heat treatment are shown in Table 2. After solution treatment at 750 °C and duplex ageing, it can be found that the strength, plasticity, and toughness of the alloy can achieve the best results. The highest fracture toughness is 101 MPa·m$^{1/2}$, the corresponding tensile strength is 1364 MPa, and the elongation is 7.8%. After solution treatment at 790 °C and duplex ageing, the strength of the alloy was the highest, the tensile strength was 1456 MPa, the corresponding elongation was 4.25%, and the fracture toughness was 78.4 MPa·m$^{1/2}$. After solution treatment at 830 °C and duplex ageing, the tensile strength was 1409 MPa, the elongation was 6.25%, and the fracture toughness was 80.2 MPa·m$^{1/2}$. In conclusion, to achieve an alloy with the best combination of high strength, high fracture toughness and good plasticity, it is necessary to rely on a combination of sparsely distributed lager α_p and dispersed needle-like α_S. The larger amount of α_p has a positive effect on the fracture toughness of the alloy, but the smaller amount of α_p can reduce the fracture toughness of the alloy, even worse than that of the alloy without α_p. The α_s that has undergone duplex aging demonstrates exceptional potential in maintaining elevated levels of strength, while simultaneously exhibiting enhancements in ductility and toughness within a specified range.

Table 2. Mechanical properties after solution treatment and duplex ageing heat treatment.

Heat Treatments	Rm (MPa)	$Rp_{0.2}$ (MPa)	A (%)	Z (%)	K_Q (MPa·m$^{1/2}$)
750 °C/0.5 h + 520 °C/4 h	1334	1304	8	24	103
750 °C/0.5 h + 520 °C/4 h + 300 °C/4 h	1364	1330	7.8	17	101
750 °C/0.5 h + 520 °C/4 h + 350 °C/4 h	1368	1332	7.5	16	96.1
750 °C/0.5 h + 520 °C/4 h + 400 °C/4 h	1373	1335	7	15	91.5
790 °C/0.5 h + 520 °C/4 h	1400	1365	7	16	84.1
790 °C/0.5 h + 520 °C/4 h + 300 °C/4 h	1417	1367	6	14.5	82.7
790 °C/0.5 h + 520 °C/4 h + 350 °C/4 h	1426	1401	5.5	11	79.5
790 °C/0.5 h + 520 °C/4 h + 400 °C/4 h	1456	1417	4.25	10.5	78.4
830 °C/0.5 h + 520 °C/4 h	1310	1252	7.75	17	88.9
830 °C/0.5 h + 520 °C/4 h + 300 °C/4 h	1330	1282	7	15	85.2
830 °C/0.5 h + 520 °C/4 h + 350 °C/4 h	1362	1289	6.5	14	84.8
830 °C/0.5 h + 520 °C/4 h + 400 °C/4 h	1409	1369	6.25	11	80.2

5. Conclusions

(1) For the solution-treated alloy, the amount of the primary α phase decreases, the size of the β grains increases with an increasing solution temperature, and the primary α phase disappears completely until 830 °C is reached. The decrease in the primary α phase results in a decrease in the strength and an increase in the plasticity, and the solution-treated alloys all have moderate strength and good plasticity.

(2) For the duplex-aged alloy, a large amount of needle-like secondary α phase is precipitated in the β matrix during the first step of ageing, resulting in an increase in the strength and a decrease in plasticity. There are finer secondary α phase precipitates between the first precipitated secondary α phase during the second step of ageing. With the increase in the second step ageing temperature, the quantity and density of the finer secondary α phase gradually increase, which causes a continuous increase in the strength and a continuous decrease in plasticity.

(3) Through duplex ageing, the microstructure consists of dense needle-like secondary α formed in the first step of ageing and more dense packing α_s precipitated in the matrix after the second step of ageing. Such a structure, in terms of the strength of the alloy, will increase the interface effect of the system and hinder the movement of dislocations to increase the strength. Regarding the fracture toughness, within a certain range, the sparsely distributed α will increase the tortuosity of the crack propagation path and enhance the fracture toughness. However, larger α_s were formed in the first step of ageing. Even if there is more intensive α_s precipitation in the second step of ageing, the overall fracture toughness of the alloy will not be seriously lost, but the second step of ageing will obviously improve the strength.

In conclusion, an excellent combination of the comprehensive properties can be achieved through solution treatment in the α/β region in addition to the descending two-step ageing.

Author Contributions: X.K.: Investigation, Validation, Writing–original draft; H.J.: Investigation, Methodology; Z.D.: Conceptuallzation, Project administration, Writing–review & editing, Supervision; T.G.: Data curation, Formal analysis; J.L. (Jingwen Liu): Methodology; W.G.: Methodology; J.C.: Investigation, Methodology; J.L. (Jingshun Liu): Investigation; G.L.: Supervision. All authors have read and agreed to the published version of the manuscript.

Funding: This research was funded by National Natural Science Foundation of China (Grant No. 52071185 and 51861029), Program for Young Talents of Science and Technology in Universities of Inner Mongolia Autonomous Region (Grant No. NJYT-19-B25), Inner Mongolia Natural Science Foundation (Grant No. 2020MS05034), Program for Innovative Research Team in Universities of Inner Mongolia Autonomous Region (Grant no. NMGIRT2211), Inner Mongolia University of Technology

Key Discipline Team Project of Materials Science (Grant no. ZD202012), Scientific Research Program of Higher Education of Inner Mongolia Autonomous Region (Grant no. NJZZ21019), Inner Mongolia Autonomous Region Natural Science Foundation (Grant No. 2021MS05009 and 2021MS05021). National Natural Science Foundation of China(52271249); Key Research and Development Program of Shaanxi(2023-YBGY-488).

Institutional Review Board Statement: Not applicable.

Informed Consent Statement: Not applicable.

Data Availability Statement: All data included in this study are available upon request by contact with the corresponding author.

Conflicts of Interest: The authors declare that they have no known competing financial interests or personal relationships that could have appeared to influence the work reported in this paper.

References

1. Kolli, R.P.; Devaraj, A. A review of metastable beta titanium alloys. *Metals* **2018**, *8*, 506. [CrossRef]
2. Yumak, N.; Aslantas, K. A review on heat treatment efficiency in metastable β titanium alloys: The role of treatment process and parameters. *J. Mater. Res. Technol.* **2020**, *9*, 15360–15380. [CrossRef]
3. Boyer, R.R.; Briggs, R.D. The use of β titanium alloys in the aerospace industry. *J. Mater. Eng. Perform.* **2013**, *22*, 2916–2920. [CrossRef]
4. Ritchie, R.O. The conflicts between strength and toughness. *Nat. Mater.* **2011**, *10*, 817–822. [CrossRef]
5. Kang, L.M.; Yang, C. A review on high-strength titanium alloys: Microstructure, strengthening, and properties. *Adv. Eng. Mater.* **2019**, *21*, 1801359. [CrossRef]
6. Cao, F.; Chandran, K.S.R.; Kumar, P. New approach to achieve high strength powder metallurgy Ti-6Al-4V alloy through accelerated sintering at β-transus temperature and hydrogenation-dehydrogenation treatment. *Scr. Mater.* **2017**, *130*, 22–26. [CrossRef]
7. Zheng, Y.F.; Williams, R.E.A.; Wang, D.; Shi, R.P.; Nag, S.; Kami, P.; Sosa, J.M.; Banerjee, R.; Wang, Y.Z.; Fraser, H.L. Role of ω phase in the formation of extremely refined intragranular α precipitates in metastable β-titanium alloys. *Acta Mater.* **2016**, *103*, 850–858. [CrossRef]
8. Lei, Z.L.; Chen, Y.; Ma, S.C.; Zhou, H.; Liu, J.T.; Wang, X.F. Influence of aging heat treatment on microstructure and tensile properties of laser oscillating welded TB8 titanium alloy joints. *Mater. Sci. Eng. A* **2020**, *797*, 140083. [CrossRef]
9. Chen, Y.Y.; Du, Z.X.; Xiao, S.L.; Xu, L.J.; Tian, J. Effect of aging heat treatment on microstructure and tensile properties of a new β high strength titanium alloy. *J. Alloys Compd.* **2014**, *586*, 588–592. [CrossRef]
10. Du, Z.X.; Xiao, S.L.; Xu, L.J.; Tian, J.; Kong, F.T.; Chen, Y.Y. Effect of heat treatment on microstructure and mechanical properties of a new β high strength titanium alloy. *Mater. Des.* **2014**, *55*, 183–190. [CrossRef]
11. Chen, K.W.; Pan, S.P.; Liu, H.Q.; Jiang, Y. Effect of α phase morphology on fatigue crack growth behavior of Ti-5Al-5Mo-5V-1Cr-1Fe alloy. *Trans. Nonferrous Met. Soc. China* **2020**, *30*, 2459–2471. [CrossRef]
12. Santhosh, R.; Geetha, M.; Saxena, V.K.; Nageswararao, M. Studies on single and duplex aging of metastable beta titanium alloy Ti-15V-3Cr-3Al-3Sn. *J. Alloys Compd.* **2014**, *605*, 222–229. [CrossRef]
13. Ren, L.; Xiao, W.L.; Han, W.Z.; Ma, C.L.; Zhou, L. Influence of duplex ageing on secondary α precipitates and mechanical properties of the near β-Ti alloy Ti-55531. *Mater. Charact.* **2018**, *144*, 1–8. [CrossRef]
14. El Chaikh, A.; Schmidt, P.; Christ, H.J. Fatigue properties of duplex-aged Ti 38-644 metastable beta titanium alloy. *Procedia Eng.* **2010**, *2*, 1973–1982. [CrossRef]
15. Ma, X.Q.; Niu, H.Z.; Yu, Z.T.; Yu, S.; Wang, C. Microstructural adjustments and mechanical properties of a cold-rolled biomedical near β-Ti alloy sheet. *Rare Met.* **2018**, *37*, 846–851. [CrossRef]
16. Liu, Z.D.; Du, Z.X.; Jiang, H.Y.; Gong, T.H.; Cui, X.M.; Liu, J.W.; Cheng, J. Microstructure evolution and corresponding tensile properties of Ti-5Al-5Mo-5V-1Cr-1Fe alloy controlling by multi-heat treatments. *Prog. Nat. Sci. Mater. Int.* **2021**, *31*, 731–741. [CrossRef]
17. Jiang, H.Y.; Du, Z.X.; Wang, D.; Gong, T.H.; Cui, X.M.; Liu, F.; Cheng, J.; Chen, W.Z. Preparation of multiscale α phase by heat treatments and its effect on tensile properties in metastable β titanium alloy a heet. *Metals* **2021**, *11*, 1708. [CrossRef]
18. Fan, J.K.; Li, J.S.; Kou, H.C.; Hua, K.; Tang, B. The interrelationship of fracture toughness and microstructure in a new near β titanium alloy Ti-7Mo-3Nb-3Cr-3Al. *Mater. Charact.* **2014**, *96*, 93–99. [CrossRef]
19. Asim, U.B.; Siddiq, M.A.; McMeeking, R.M.; Kartal, M.E. A multiscale constitutive model for metal forming of dual phase titanium alloys by incorporating inherent deformation and failure mechanisms. *Model. Simul. Mater. Sci. Eng.* **2022**, *30*, 025008. [CrossRef]
20. Wang, H.; Zhao, Q.Y.; Xin, S.W.; Zhao, Y.Q.; Zhou, W.; Zeng, W.D. Microstructural morphology effects on fracture toughness and crack growth behaviors in a high strength titanium alloy. *Mater. Sci. Eng. A* **2021**, *821*, 141626. [CrossRef]
21. Zhu, W.G.; Lei, J.; Su, B.; Sun, Q.Y. The interdependence of microstructure, strength and fracture toughness in a novel β titanium alloy Ti-5Al-4Zr-8Mo-7V. *Mater. Sci. Eng. A* **2020**, *782*, 139248. [CrossRef]

22. Zhu, W.G.; Lei, J.; Tan, C.S.; Sun, Q.Y.; Chen, W.; Xiao, L.; Sun, J. A novel high-strength β-Ti alloy with hierarchical distribution of α-phase: The superior combination of strength and ductility. *Mater. Des.* **2019**, *168*, 107640. [CrossRef]
23. Issariyapat, A.; Visuttipitukul, P.; Song, T.T.; Bahador, A.; Umeda, J.; Qian, M.; Kondoh, K. Tensile properties improvement by homogenized nitrogen solid solution strengthening of commercially pure titanium through powder metallurgy process. *Mater. Charact.* **2020**, *170*, 110700. [CrossRef]
24. Jia, M.T.; Zhang, D.L.; Gabbitas, B.; Liang, J.M.; Kong, C. A novel Ti-6Al-4V alloy microstructure with very high strength and good ductility. *Scr. Mater.* **2015**, *107*, 10–13. [CrossRef]
25. Liu, Z.D.; Du, Z.X.; Jiang, H.Y.; Zhao, X.P.; Gong, T.H.; Cui, X.M.; Cheng, J.; Liu, F.; Chen, W.Z. Controlling the microstructure and fracture toughness of the Ti-5Al-5Mo-5V-1Cr-1Fe alloy by multiple heat treatments. *J. Mater. Res. Technol.* **2022**, *17*, 2528–2539. [CrossRef]
26. Lu, J.W.; Zhao, Y.Q.; Ge, P.; Niu, H.Z.; Zhang, Y.S.; Zhang, W.; Zhang, P.X. Microstructure and mechanical properties of new high strength beta-titanium alloy Ti-1300. *Mater. Sci. Eng. A* **2015**, *621*, 182–189. [CrossRef]
27. Chaudhuri, K.; Perepezko, J.H. Microstructural study of the titanium alloy Ti-15Mo-2.7Nb-3Al-0.2Si (TIMETAL 21S). *Metall. Mater. Trans. A* **1994**, *25*, 1109–1118. [CrossRef]
28. Wang, Z.Y.; Liu, L.B.; Zhang, L.G.; Sheng, J.W.; Wu, D.; Yuan, M.W. Effect of heat treatment on the microstructure and mechanical properties of high-strength Ti-6Al-4V-5Fe alloy. *Mater. Trans.* **2019**, *60*, 269–276. [CrossRef]
29. Li, C.L.; Mi, X.J.; Ye, W.J.; Hui, S.X.; Yu, Y.; Wang, W.Q. A study on the microstructures and tensile properties of new beta high strength titanium alloy. *J. Alloys Compd.* **2013**, *550*, 23–30. [CrossRef]
30. Ivasishin, O.M.; Markovsky, P.E.; Semiatin, S.L.; Ward, C.H. Aging response of coarse- and fine-grained titanium alloys. *Mater. Sci. Eng. A* **2005**, *405*, 296–305. [CrossRef]
31. Liu, Y.; Lim, S.C.V.; Ding, C.; Huang, A.J.; Weyland, M. Unravelling the competitive effect of microstructural features on the fracture toughness and tensile properties of near beta titanium alloys. *J. Mater. Sci. Technol.* **2022**, *97*, 101–112. [CrossRef]
32. Tan, C.S.; Sun, Q.Y.; Xiao, L.; Zhao, Y.Q.; Sun, J. Characterization of deformation in primary α phase and crack initiation and propagation of TC21 alloy using in-situ SEM experiments. *Mater. Sci. Eng. A* **2018**, *725*, 33–42. [CrossRef]
33. Terlinde, G.; Schwalbe, H.J.; Schwalbe, K.H. Microstructure and fracture toughness of the aged, β-Ti alloy Ti-10V-2Fe-3Al. *Metall. Trans. A* **1988**, *19*, 1037–1049. [CrossRef]
34. Shi, X.H.; Zeng, W.D.; Shi, C.L.; Wang, H.J.; Jia, Z.Q. The fracture toughness and its prediction model for Ti-5Al-5Mo-5V-1Cr-1Fe titanium alloy with basket-weave microstructure. *J. Alloys Compd.* **2015**, *632*, 748–755. [CrossRef]
35. Bhattacharjee, A.; Varma, V.K.; Kamat, S.V.; Gogia, A.K.; Bhargava, S. Influence of β grain size on tensile behavior and ductile fracture toughness of titanium alloy Ti-10V-2Fe-3Al. *Metall. Mater. Trans. A* **2006**, *37*, 1423–1433. [CrossRef]
36. Ghosh, A.; Sivaprasad, S.; Bhattacharjee, A.; Kar, S.K. Microstructure-fracture toughness correlation in an aircraft structural component alloy Ti-5Al-5V-5Mo-3Cr. *Mater. Sci. Eng. A* **2013**, *568*, 61–67. [CrossRef]
37. Wang, H.; Xin, S.W.; Zhao, Y.Q.; Zhou, W.; Zeng, W.D. Plane strain fracture behavior of a new high strength Ti-5Al-3Mo-3V-2Zr-2Cr-1Nb-1Fe alloy during heat treatment. *Mater. Sci. Eng. A* **2020**, *797*, 140080. [CrossRef]
38. Mora, L.; Quesne, C.; Penelle, R. Relationships among thermomechanical treatments, microstructure, and tensile properties of a near beta-titanium alloy: β-CEZ: Part II. Relationships between thermomechanical treatments and tensile properties. *J. Mater. Res.* **1996**, *11*, 89–99. [CrossRef]
39. Wu, C.; Zhan, M. Effect of solution plus aging heat treatment on microstructural evolution and mechanical properties of near-β titanium alloy. *Trans. Nonferrous Met. Soc. China* **2019**, *29*, 997–1006. [CrossRef]
40. Mine, Y.; Takashima, K.; Bowen, P. Effect of lamellar spacing on fatigue crack growth behaviour of a TiAl-based aluminide with lamellar microstructure. *Mater. Sci. Eng. A* **2012**, *532*, 13–20. [CrossRef]

Disclaimer/Publisher's Note: The statements, opinions and data contained in all publications are solely those of the individual author(s) and contributor(s) and not of MDPI and/or the editor(s). MDPI and/or the editor(s) disclaim responsibility for any injury to people or property resulting from any ideas, methods, instructions or products referred to in the content.